UNIVERSITY OF AMSTERDAM

UvA-DARE (Digital Academic Repository)

Super-Eddington Accretion Geometry

A Remarkable Stability of the Hidden Ultraluminous X-Ray Source Cygnus X-3

Ng, Chi-Yung; IXPE

DOI
10.3847/1538-4357/ae7366

Publication date
2026

Document Version
Final published version

Published in
Astrophysical Journal

License
CC BY

Link to publication

Citation for published version (APA):
Ng, C.-Y., & IXPE (2026). Super-Eddington Accretion Geometry: A Remarkable Stability of the Hidden Ultraluminous X-Ray Source Cygnus X-3. *Astrophysical Journal*, *1005*(1), Article 83. https://doi.org/10.3847/1538-4357/ae7366

General rights
It is not permitted to download or to forward/distribute the text or part of it without the consent of the author(s) and/or copyright holder(s), other than for strictly personal, individual use, unless the work is under an open content license (like Creative Commons).

Disclaimer/Complaints regulations
If you believe that digital publication of certain material infringes any of your rights or (privacy) interests, please let the Library know, stating your reasons. In case of a legitimate complaint, the Library will make the material inaccessible and/or remove it from the website. Please Ask the Library: https://uba.uva.nl/en/contact, or a letter to: Library of the University of Amsterdam, Secretariat, P.O. Box 19185, 1000 GD Amsterdam, The Netherlands. You will be contacted as soon as possible.

UvA-DARE is a service provided by the library of the University of Amsterdam (https://dare.uva.nl)

Download date:10 Oct 2026

The Astrophysical Journal, 1005:83 (9pp), 2026 July 1 https://doi.org/10.3847/1538-4357/ae7366
© 2026. The Author(s). Published by the American Astronomical Society.
OPEN ACCESS

Super-Eddington Accretion Geometry: A Remarkable Stability of the Hidden Ultraluminous X-Ray Source Cygnus X-3

Romana Mikušincová[1], Alexandra Veledina[2,3], Fabio Muleri[1], Raul Ciancarella[4], Andrzej Zdziarski[5], David A. Green[6], Michael McCollough[7], Henric Krawczynski[8], James F. Steiner[9], Michal Dovčiak[10], Varpu Ahlberg[2], Stefano Bianchi[11], Alessandro Di Marco[1], Javier A. García[12], Adam Ingram[13], Philip Kaaret[14], Timothy Kallman[12], Hu Kun[8], Fabio La Monaca[1,15], Alexander Lange[16], Vladislav Loktev[13], Guglielmo Mastroserio[17], Giorgio Matt[11], Razieh Emami[9], Pierre-Olivier Petrucci[18], Jakub Podgorný[10], Juri Poutanen[2], Ajay Ratheesh[1,19], Nicole Rodriguez[8], Jiří Svoboda[10], Francesco Tombesi[20,21,22], Francesco Ursini[11], Iván Agudo[23], Lucio A. Antonelli[22,24], Matteo Bachetti[25], Luca Baldini[26,27], Wayne H. Baumgartner[28], Ronaldo Bellazzini[26], Stephen D. Bongiorno[14], Raffaella Bonino[29,30], Alessandro Brez[26], Niccolò Bucciantini[31,32,33], Fiamma Capitanio[1], Simone Castellano[26], Elisabetta Cavazzuti[34], Chien-Ting Chen[35], Stefano Ciprini[24,36], Enrico Costa[1], Alessandra De Rosa[1], Ettore Del Monte[1], Laura Di Gesu[34], Niccolò Di Lalla[37], Immacolata Donnarumma[34], Victor Doroshenko[38], Steven R. Ehlert[14], Teruaki Enoto[39], Yuri Evangelista[1], Sergio Fabiani[1], Riccardo Ferrazzoli[1], Shuichi Gunji[40], Kiyoshi Hayashida[41,62], Jeremy Heyl[42], Wataru Iwakiri[43], Svetlana G. Jorstad[44,45], Vladimir Karas[10], Fabian Kislat[46], Takao Kitaguchi[39], Jeffery J. Kolodziejczak[14], Luca Latronico[29], Ioannis Liodakis[47], Simone Maldera[29], Alberto Manfreda[48], Frédéric Marin[49], Andrea Marinucci[34], Alan P. Marscher[44], Herman L. Marshall[50], Francesco Massaro[29,30], Ikuyuki Mitsuishi[51], Tsunefumi Mizuno[52], Michela Negro[53], Chi- Yung Ng[54], Stephen L. O'Dell[14], Nicola Omodei[37], Chiara Oppedisano[29], Alessandro Papitto[22], George G. Pavlov[55], Abel L. Peirson[37], Matteo Perri[22,24], Melissa Pesce-Rollins[26], Maura Pilia[25], Andrea Possenti[25], Simonetta Puccetti[24], Brian D. Ramsey[14], John Rankin[56], Oliver J. Roberts[35], Roger W. Romani[37], Carmelo Sgrò[26], Patrick Slane[57], Paolo Soffitta[1], Gloria Spandre[26], Douglas A. Swartz[35], Toru Tamagawa[39], Fabrizio Tavecchio[56], Roberto Taverna[58], Yuzuru Tawara[51], Allyn F. Tennant[14], Nicholas E. Thomas[14], Alessio Trois[25], Sergey S. Tsygankov[2], Roberto Turolla[58,59], Jacco Vink[60], Martin C. Weisskopf[14], Kinwah Wu[59], Fei Xie[1,61], and Silvia Zane[59]

[1] INAF Istituto di Astrofisica e Planetologia Spaziali, Via del Fosso del Cavaliere 100, 00133 Roma, Italy; romana.mikusincova@inaf.it
[2] Department of Physics and Astronomy, 20014, University of Turku, Finland
[3] Nordita, KTH Royal Institute of Technology and Stockholm University, Hannes Alfvéns väg 12, SE-10691 Stockholm, Sweden
[4] Independent Researcher
[5] Nicolaus Copernicus Astronomical Center, Polish Academy of Sciences, Bartycka 18, PL–00–716 Warszawa, Poland
[6] Astrophysics Group, Cavendish Laboratory, J. J. Thomson Avenue, Cambridge CB3 0US, UK
[7] Harvard-Smithsonian Center for Astrophysics, 60 Garden Street, Cambridge, MA 02138, USA
[8] Physics Department and McDonnell Center for the Space Sciences, Washington University in St. Louis, St. Louis, MO 63130, USA
[9] Center for Astrophysics, Harvard & Smithsonian, Cambridge, MA 02138, USA
[10] Astronomical Institute of the Czech Academy of Sciences, Boční II 1401/1, 14100, Praha 4, Czechia
[11] Dipartimento di Matematica e Fisica, Università degli Studi Roma Tre, Via della Vasca Navale 84, 00146 Roma, Italy
[12] X-ray Astrophysics Laboratory, NASA Goddard Space Flight Center, Greenbelt, MD 20771, USA
[13] School of Mathematics, Statistics, and Physics, Newcastle University, Newcastle upon Tyne NE1 7RU, UK
[14] NASA Marshall Space Flight Center, Huntsville, AL 35812, USA
[15] Dipartimento di Fisica, Università degli Studi di Roma "Tor Vergata", Via della Ricerca Scientifica 1, 00133, Rome, Italy
[16] Department of Physics, The George Washington University, 725 21st Street NW, Washington, DC 20052, USA
[17] Scuola Universitaria Superiore IUSS Pavia, Palazzo del Broletto, piazza della Vittoria 15, I-27100 Pavia, Italy
[18] Université Grenoble Alpes, CNRS, IPAG, 38000 Grenoble, France
[19] Physical Research Laboratory, Thaltej, Ahmedabad, Gujarat 380009, India
[20] Tor Vergata University of Rome, Via Della Ricerca Scientifica 1, 00133 Rome, Italy
[21] INFN—Rome Tor Vergata, Via della Ricerca Scientifica 1, 00133 Rome, Italy
[22] INAF Osservatorio Astronomico di Roma, Via Frascati 33, 00078, Monte Porzio Catone (RM), Italy
[23] Instituto de Astrofísica de Andalucía—CSIC, Glorieta de la Astronomía s/n, 18008 Granada, Spain
[24] Space Science Data Center, Agenzia Spaziale Italiana, Via del Politecnico snc, 00133 Roma, Italy
[25] INAF Osservatorio Astronomico di Cagliari, Via della Scienza 5, 09047, Selargius (CA), Italy
[26] Istituto Nazionale di Fisica Nucleare, Sezione di Pisa, Largo B. Pontecorvo 3, 56127 Pisa, Italy
[27] Dipartimento di Fisica, Università di Pisa, Largo B. Pontecorvo 3, 56127 Pisa, Italy
[28] Naval Research Laboratory, 4555 Overlook Avenue SW, WA, DC 20375, USA
[29] Istituto Nazionale di Fisica Nucleare, Sezione di Torino, Via Pietro Giuria 1, 10125 Torino, Italy
[30] Dipartimento di Fisica, Università degli Studi di Torino, Via Pietro Giuria 1, 10125 Torino, Italy
[31] INAF Osservatorio Astrofisico di Arcetri, Largo Enrico Fermi 5, 50125 Firenze, Italy
[32] Dipartimento di Fisica e Astronomia, Università degli Studi di Firenze, Via Sansone 1, 50019, Sesto Fiorentino (FI), Italy
[33] Istituto Nazionale di Fisica Nucleare, Sezione di Firenze, Via Sansone 1, 50019, Sesto Fiorentino (FI), Italy
[34] Agenzia Spaziale Italiana, Via del Politecnico snc, 00133 Roma, Italy
[35] Science and Technology Institute, Universities Space Research Association, Huntsville, AL 35805, USA
[36] Istituto Nazionale di Fisica Nucleare, Sezione di Roma "Tor Vergata", Via della Ricerca Scientifica 1, 00133 Roma, Italy
[37] Department of Physics and Kavli Institute for Particle Astrophysics and Cosmology, Stanford University, Stanford, CA 94305, USA
[38] Institut für Astronomie und Astrophysik, Universität Tübingen, Sand 1, 72076, Tübingen, Germany
[39] RIKEN Cluster for Pioneering Research, 2-1 Hirosawa, Wako, Saitama 351-0198, Japan
[40] Yamagata University, 1-4-12 Kojirakawa-machi, Yamagata-shi 990-8560, Japan

[41] Osaka University, 1-1 Yamadaoka, Suita, Osaka 565-0871, Japan
[42] University of British Columbia, Vancouver, BC V6T 1Z4, Canada
[43] International Center for Hadron Astrophysics, Chiba University, Chiba 263-8522, Japan
[44] Institute for Astrophysical Research, Boston University, 725 Commonwealth Avenue, Boston, MA 02215, USA
[45] Department of Astrophysics, St. Petersburg State University, Universitetsky pr. 28, Petrodvoretz, 198504, St. Petersburg, Russia
[46] Department of Physics and Astronomy and Space Science Center, University of New Hampshire, Durham, NH 03824, USA
[47] Institute of Astrophysics, FORTH, N. Plastira 100, GR-70013 Vassilika Vouton, Greece
[48] Istituto Nazionale di Fisica Nucleare, Sezione di Napoli, Strada Comunale Cinthia, 80126 Napoli, Italy
[49] Université de Strasbourg, CNRS, Observatoire Astronomique de Strasbourg, UMR 7550, 67000 Strasbourg, France
[50] MIT Kavli Institute for Astrophysics and Space Research, Massachusetts Institute of Technology, 77 Massachusetts Avenue, Cambridge, MA 02139, USA
[51] Graduate School of Science, Division of Particle and Astrophysical Science, Nagoya University, Furo-cho, Chikusa-ku, Nagoya, Aichi 464-8602, Japan
[52] Hiroshima Astrophysical Science Center, Hiroshima University, 1-3-1 Kagamiyama, Higashi-Hiroshima, Hiroshima 739-8526, Japan
[53] Department of Physics and Astronomy, Louisiana State University, Baton Rouge, LA 70803, USA
[54] Department of Physics, The University of Hong Kong, Pokfulam, Hong Kong
[55] Department of Astronomy and Astrophysics, Pennsylvania State University, University Park, PA 16801, USA
[56] INAF Osservatorio Astronomico di Brera, Via E. Bianchi 46, 23807, Merate (LC), Italy
[57] Center for Astrophysics, Harvard & Smithsonian, 60 Garden Street, Cambridge, MA 02138, USA
[58] Dipartimento di Fisica e Astronomia, Università degli Studi di Padova, Via Marzolo 8, 35131 Padova, Italy
[59] Mullard Space Science Laboratory, University College London, Holmbury St Mary, Dorking, Surrey RH5 6NT, UK
[60] Anton Pannekoek Institute for Astronomy & GRAPPA, University of Amsterdam, Science Park 904, 1098 XH Amsterdam, The Netherlands
[61] Guangxi Key Laboratory for Relativistic Astrophysics, School of Physical Science and Technology, Guangxi University, Nanning 530004, People's Republic of China

Received 2025 September 8; revised 2026 May 14; accepted 2026 May 25; published 2026 June 26

Abstract

We report on the average and orbital phase-resolved polarization of Cyg X-3 in the hard state (HS) during the 2023 Imaging X-ray Polarimetry Explorer (IXPE) observational campaign. We find the polarization degree of $21.4\% \pm 0.4\%$ and polarization angle of $92.^{\circ}2 \pm 0.^{\circ}5$, compatible within 3σ with the first HS IXPE observation in 2022. As the observed polarization depends on both the accretion geometry and the X-ray emission mechanism, and assuming it arises from reflection from the optically thick envelope surrounding the central source, our result indicates that both are similar in the two HS epochs on year-long timescales despite the source transitioning through an intermediate state in between. We discuss time- and energy-dependent polarization properties and their implications for the geometry and stability of the accretion funnel, finding significant orbital modulation of the polarization properties.

Unified Astronomy Thesaurus concepts: Accretion (14); Polarimetry (1278); X-ray astronomy (1810); X-ray binary stars (1811); Stellar mass black holes (1611)

1. Introduction

Cygnus X-3 (hereafter Cyg X-3) is a persistent radio, X-ray, and γ-ray source and a high-mass X-ray binary system composed of a compact object, likely being a neutron star or a low-mass black hole (BH; A. A. Zdziarski et al. 2013), and a Wolf–Rayet star (M. H. van Kerkwijk et al. 1996). The findings of A. A. Zdziarski et al. (2013) of a low-mass BH are different from those of I. I. Antokhin et al. (2022), who favored $\sim 7\,M_{\odot}$. However, new research based on XRISM results (D. Miura et al. 2025) finds results very similar to the earlier findings. The orbital period of Cyg X-3 is $P \approx 4.8$ hr (D. R. Parsignault et al. 1972), which is among the shortest known for X-ray binaries. Interestingly, since its discovery (R. Giacconi et al. 1967), the source has been known to exhibit peculiar multiwavelength properties. In fact, Cyg X-3 has attracted particular interest since the first observation of its radio flares (P. C. Gregory et al. 1972), when it became the brightest X-ray binary in radio with flux density reaching 20 Jy (e.g., M. L. McCollough et al. 1999; S. Corbel et al. 2012; R. E. Spencer et al. 2022).

The source is also atypically bright in the γ-rays (W. B. Atwood et al. 2009; M. Tavani et al. 2009), suggesting that a peculiar accretion geometry might be favoring the conditions for launching truly powerful outflows. Cyg X-3 exhibits transient γ-ray emission above 100 MeV, firmly detected by AGILE and Fermi-LAT (A. A. Abdo et al. 2009; M. Tavani et al. 2009). These γ-ray episodes occur when the system is in the soft X-ray spectral state and just before major radio flares, with the peak isotropic luminosity reaching $\sim 10^{36}$ erg s^{-1}, assuming a distance of 7–10 kpc. More recent findings by M. J. Reid & J. C. A. Miller-Jones (2023) constrain the distance to 9–10 kpc. The γ-ray spectrum is well described by a power law $dN/dE \propto E^{-\Gamma}$ with a photon index $\Gamma \sim 2$ (G. Piano et al. 2012), and the emission is modulated on the 4.8 hr orbital period, suggesting an origin in the relativistic jet at distances of $\sim 10^{10}$–$\sim 3 \times 10^{12}$ cm from the compact object (G. Dubus et al. 2010; B. Cerutti et al. 2011).

X-ray polarimetric studies, enabled by the Imaging X-ray Polarimetry Explorer (IXPE; P. Soffitta et al. 2021; M. C. Weisskopf et al. 2022), offer a novel diagnostic that can resolve longstanding uncertainties about the geometry of the emission region. IXPE can measure the linear polarization in the 2–8 keV energy range, providing space-resolved (with $\sim 30''$ half-power diameter) and energy-resolved (resolution better than 20% at 6 keV) observations. Several X-ray binary systems (M. Dovčiak et al. 2024) were found to have a high (between about 3% and 12%) polarization degree (PD) in the hard spectral state: Cyg X-1 (H. Krawczynski et al. 2022;

[62] Deceased.

Original content from this work may be used under the terms of the Creative Commons Attribution 4.0 licence. Any further distribution of this work must maintain attribution to the author(s) and the title of the work, journal citation and DOI.

V. Kravtsov et al. 2025), Swift J1727.8−1613 (A. Veledina et al. 2023; A. Ingram et al. 2024; J. Podgorný et al. 2024), and IGR J17091−3624 (M. Ewing et al. 2025), with the polarization angle (PA) coinciding with the position angle of the jet (which is also aligned with the optical polarization). These results have been interpreted in terms of the hot, X-ray-emitting medium being elongated in the disk plane. The hard-state (HS) geometry remains stable despite X-ray flux variations spanning up to 2 orders of magnitude (J. Podgorný et al. 2024; V. Kravtsov et al. 2025). The results for Cyg X-1 and IGR J1709−3624 may require the Comptonizing medium to move at half the speed of light to explain the high PD values (A. M. Beloborodov 1998; J. Poutanen et al. 2023; H. Krawczynski & K. Hu 2025).

The spectral states of Cyg X-3 are similar to other X-ray binary systems harboring BHs (A. Szostek et al. 2008). The source switches spectral states in a known, repeating manner, with the X-ray spectral states being tightly related to the radio properties. It is most often found in the hard X-ray, quiescent radio state, in which the X-ray spectrum is dominated by a power-law-like continuum with a prominent reflection complex (e.g., L. Hjalmarsdotter et al. 2008), and the flux density in radio bands is ∼100 mJy (e.g., M. L. McCollough et al. 1999; S. Trushkin et al. 2017). Incursions into the X-ray intermediate state (IMS) are accompanied by an increase of radio flux densities up to ∼0.3 Jy and softening of the X-ray spectrum. The IMS is sometimes followed by a transition to the ultrasoft X-ray (SS), quenched radio state, with a blackbody-like spectrum and low levels of radio flux density $\lesssim$10 mJy. After that, the source shows major radio ejections and closes the activity loop by returning to the HS. Each spectral state typically lasts from several weeks to a few months, as observed in long-term monitoring with the Swift Burst Alert Telescope observatory.

The physical mechanism of the repeating spectral state changes observed over long timescales in X-ray and radio properties of Cyg X-3 is not known. Potential scenarios include changes of the local absorption (L. Hjalmarsdotter et al. 2009), the transformation of the funnel-like accretion geometry into disk-dominated accretion, akin to typical low-mass BH X-ray binaries in the soft spectral state, or the repeating filling of an inner funnel with matter and its subsequent clearing (A. Veledina et al. 2024b). Recent IXPE polarimetric observations have indeed revealed evidence for an atypical geometry in Cyg X-3 (A. Veledina et al. 2024a, 2024b). The distinct HS spectra of the source, closely resembling reflected emission, and the exceptionally high PD ∼20% orthogonal to the direction of radio ejections are reminiscent of those detected in obscured Seyfert 2 galaxies (e.g., F. Ursini et al. 2023). These properties favor a geometry where the source of the incident X-ray emission is covered by a thick conical structure located high above the orbital plane. At an inclination of 30° (A. Veledina et al. 2024a, 2024b), this structure blocks direct radiation from the line of sight, and the observer sees only reflected emission from its inner walls. The inferred luminosity, both intrinsic and apparent for the observer looking down the funnel, appeared to exceed 3×10^{39} erg s^{-1}, rendering Cyg X-3 in the class of ultraluminous X-ray sources (ULXs) and then the first source of this kind studied through X-ray polarimetric analysis.

A clue to this puzzle is an important constraint of accretion geometry: if a substantial fraction of the funnel material is blown away together with the major radio ejection, one may expect the gradual accumulation of matter during episodes of quiescent radio emission until the subsequent ejection. Parameters of the funnel, such as the size, optical thickness, and opening angle, determine the beaming factor and hence the brightness of this off-axis ULX. Variations in the opening angle would manifest themselves in changes of the apparent luminosity, while the size of the funnel proportionally affects the amount of observed radiation. Previous findings by A. Veledina et al. (2024a) constrained the opening angle in the HS $\lesssim$15°.

In this paper, we explore the long-term evolution of the accretion geometry of Cyg X-3 in the hard X-ray spectral state. IXPE observed Cyg X-3 in 2023 November, about 1 yr after the first HS observation of the source. In this paper, we report on the observed average and orbital phase-resolved polarimetric properties of the source. We describe the data reduction in Section 2. The results of data analysis and their implications for the properties of the system are presented in Section 3. We summarize our findings in Section 4. In line with the current consensus, in this work, we assume that Cyg X-3 harbors a BH.

2. Observation and Methods

Cyg X-3 was observed by IXPE during four epochs in total so far. All of the observations are reported in Table 1. Over these epochs, the source was caught in three spectral states showing different polarization properties. The HS shows a prominent PD of ∼20%, higher than the SS and IMS. The latter two differ by only $\Delta\mathrm{PD} \sim 1.5\%$. On the other hand, PA stays constant within 3σ between all of the observations.

Here we focus on the third observation of Cyg X-3 (Observation ID 02009101, hereafter referred to as HS 2023), which took place between 2023 November 17 (start time 20:16:16 UTC) and 2023 November 23 (end time 23:08:15 UTC) for approximately 291 ks, and compare it with the other three IXPE observations of the source. We downloaded the Level 2 data from the public HEASARC data archive and proceeded with the data reduction. The `barycorr` tool, from the FTOOLS package (HEASOFT software version 6.35.1), was applied to the data in order to adjust the timing of the events' arrival relative to the solar system's barycenter. We used the IXPEOBSSIM software (v. 31.0.1; L. Baldini et al. 2022) and its `xpselect` feature to select the source region. The extraction regions were circular with a radius of 90″. Since the source is very bright (>2 counts s^{-1}), no background rejection or subtraction was necessary (A. Di Marco et al. 2023). The `xpbin` tool of IXPEOBSSIM was used to create the polarization cubes (`pcube`) as well as to generate the *I*, *Q*, and *U* Stokes spectra. In the end, the `ftgrouppha` (FTOOLS) was used to rebin the Stokes spectra to contain eight counts per bin for Stokes *I*, *Q*, and *U*. Version 20230101_v013 of the response matrices was used to create these products, applying unweighted (`pcube`) and weighted (Stokes *I*, *Q*, *U*) analysis (A. Di Marco et al. 2022).

It is well established that the source undergoes pronounced flux modulation with the orbital phase of the binary system (I. I. Antokhin et al. 2022). Also, the source showed orbital variations of the X-ray polarization during the first two observations carried out by IXPE (A. Veledina et al. 2024a).

Data from HS 2023 are therefore phase-folded based on the quadratic ephemeris model presented in Table 2 of

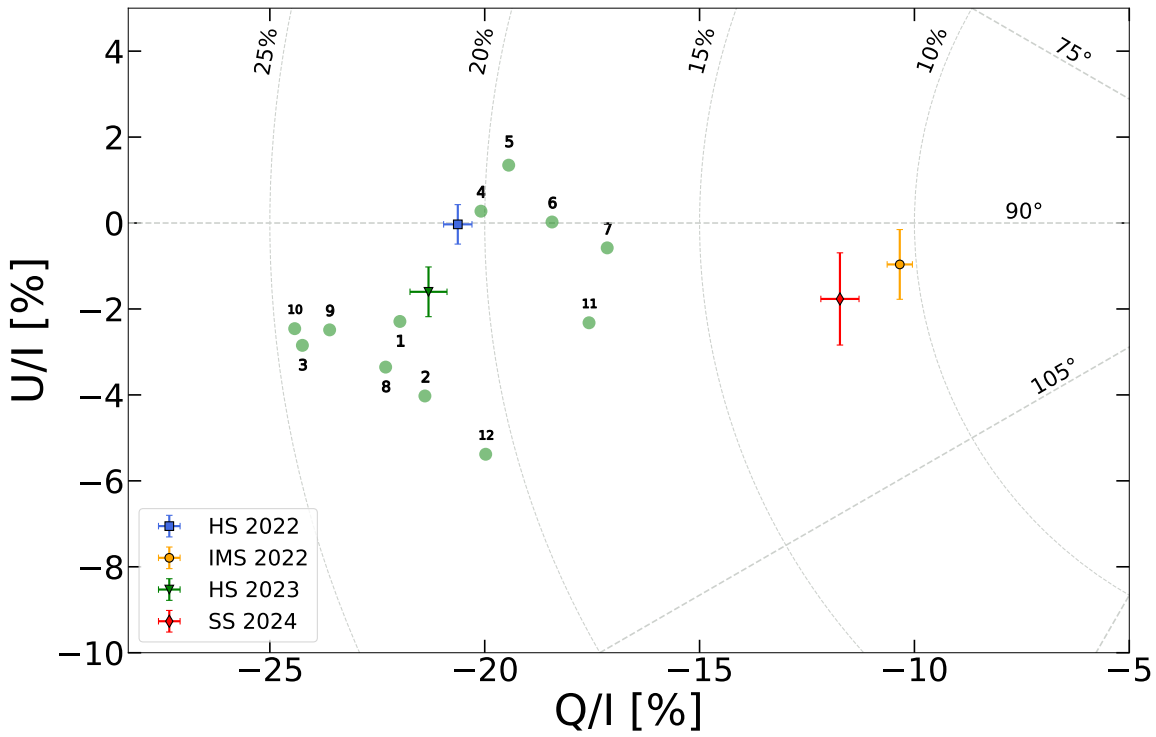

Figure 1. Normalized Stokes parameters U/I versus Q/I for the IXPE observations of Cyg X-3. HS 2022 in blue, IMS 2022 in yellow, HS 2023 in green, and SS 2024 in red. The error bars are plotted at 1σ CL. In the case of HS 2023, we also plot the change of the polarization properties with the orbital phase in fainter green, numbered 1–12, with bin 1 centered on phase 0. The light-green points are shown without error bars, which are on average $\Delta(Q/I) \approx \Delta(U/I) \approx 2\%$ ($1\,\sigma$). The gray grid represents the PD (in percent) and PA (in degrees).

Table 1
Observations of Cyg X-3 Performed by IXPE and Its Measured Polarimetric Properties in Their Respective Spectral States

Obs ID	Start Date	End Date	Exposure (ks)	Spectral State	PD (%)	PA (deg)	ID
02001899	2022-10-14	2022-11-06	538	HS	20.6 ± 0.3	90.1 ± 0.4	HS 2022
02250301	2022-12-25	2022-12-29	199	IMS	10.4 ± 0.3	92.6 ± 0.7	IMS 2022
02009101	2023-11-17	2023-11-23	291	HS	21.4 ± 0.4	92.2 ± 0.5	HS 2023
03250301	2024-06-02	2024-06-03	50	SS	11.9 ± 0.4	94.0 ± 1.0	SS 2024

Note. Uncertainties at 1σ CL. Observation HS 2023 is the main focus of this paper. HS 2022 and IMS 2022 are discussed in A. Veledina et al. (2024a), SS 2024 in A. Veledina et al. (2024b), and N. Rodriguez-Cavero et al. 2026 (in preparation). We define the reference ID for each observation in the last column and adopt this notation throughout the paper.

I. I. Antokhin & A. M. Cherepashchuk (2019), where phase 0 corresponds to the superior conjunction of the system.

We then calculated the phase of each detected event and added this information to the data file. We split the observation into 12 phase bins, with phase 0 defined as the center of the first bin.

3. Results

3.1. Energy-dependent Polarimetry

Using the `pcube` algorithm of IXPEOBSSIM to determine the presence of model-independent polarization, we obtain the values of energy-averaged PD and PA, which are depicted in Figure 1. During HS 2023, the source shows high PD=21.4% ± 0.4% at PA=92°.2 ± 0°.5 (hereafter errors are quoted at the 68.3% confidence level; CL). Over the IXPE observations of Cyg X-3 conducted so far, the PA has shown almost no variation, whereas the PD has exhibited substantial changes (see Table 1). There is a difference of $\Delta\mathrm{PD} \sim 10\%$ between the PD in the HS (HS 2022 and HS 2023) versus IMS (IMS 2022) and SS (SS 2024). Interestingly, the IMS and SS differ by only ΔPD=1.5% ± 0.5%. The PD values in HS 2022 and HS 2023 differ by ΔPD=0.8% ± 0.5% ($1\,\sigma$).

In Figure 2, we show the energy dependence of the polarization properties for the four observations. Over the entire 2–8 keV wave band, both PD and PA do not exhibit large variations, although some minor changes are observed, especially in the case of PD. In particular, there is a slight increase in PD in the energy range 2–5 keV followed by a moderate decrease as we reach 8 keV (HS 2022 and HS 2023), which is due to the presence of prominent iron lines. In a recent paper using high-resolution XRISM spectroscopy, M. Audard et al. (2024) have confirmed this to be a group of fluorescence lines caused by different ionization states of the element, which are expected to be unpolarized. The initial PD growth with energy does not seem to be present in the IMS and SS. The PA shows a more constant trend across the IXPE energy band in all four of the observations.

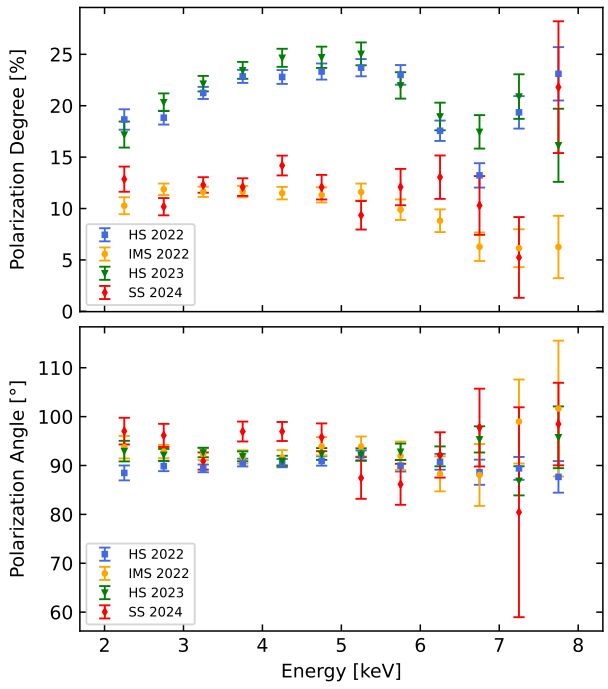

Figure 2. Dependence of PD (top) and PA (bottom) on energy in the 2–8 keV band. HS 2022 in blue squares, IMS 2022 in yellow circles, HS 2023 in green triangles, and SS 2024 in red diamonds.

The energy dependence of the Stokes parameters I, Q, and U in the two HS observations, HS 2022 and HS 2023, is shown in Figure 3. The main difference between the two observations is seen from the spectral shape of the Stokes I datasets, particularly at lower energies, where we notice a softer spectra in the case of HS 2023.

3.2. Polarization in the Hard Spectral State

Although the polarization of the source in HS 2023 is comparable to that of HS 2022, they are not identical. The difference can be noticed in the spectral dependence of the PD (Figure 2) found by fitting the PD data obtained from the `pcube` using models with a linear energy-dependent PD and a nonpolarized Gaussian versus constant polarization with a nonpolarized Gaussian (Figure 4). The peak of the Gaussian was fixed at 6.7 keV, as that is the energy of Fe XXV—the iron type with the highest equivalent width found in the Cyg X-3 spectra (extended data Figure 6 of A. Veledina et al. 2024a). The fit with linear energy-dependent PD is significantly favored, with a χ^2/d.o.f. $= 10.2/8$ (HS 2022) and a χ^2/d.o.f. $= 14.8/8$ (HS 2023), compared to χ^2/d.o.f. $= 47.0/9$ (HS 2022) and χ^2/d.o.f. $= 44.3/9$ (HS 2023) for the constant PD model. These results correspond to improvements of $\approx 4\sigma$ (p-value of 6×10^{-4}) and $\approx 3.5\sigma$ ($p = 4 \times 10^{-3}$), respectively. This could indicate a suppression of polarization at low energies in HS 2023, which may come from a possible joint contribution of abundant emission lines (seen in Chandra; T. Kallman et al. 2019), although their relative contribution within the IXPE energy band is not directly constrained here, the unpolarized contribution of the reprocessed emission from the funnel walls, or from the scattered light from the central source within the funnel (polarized at ∼10%; A. Veledina et al. 2024b).

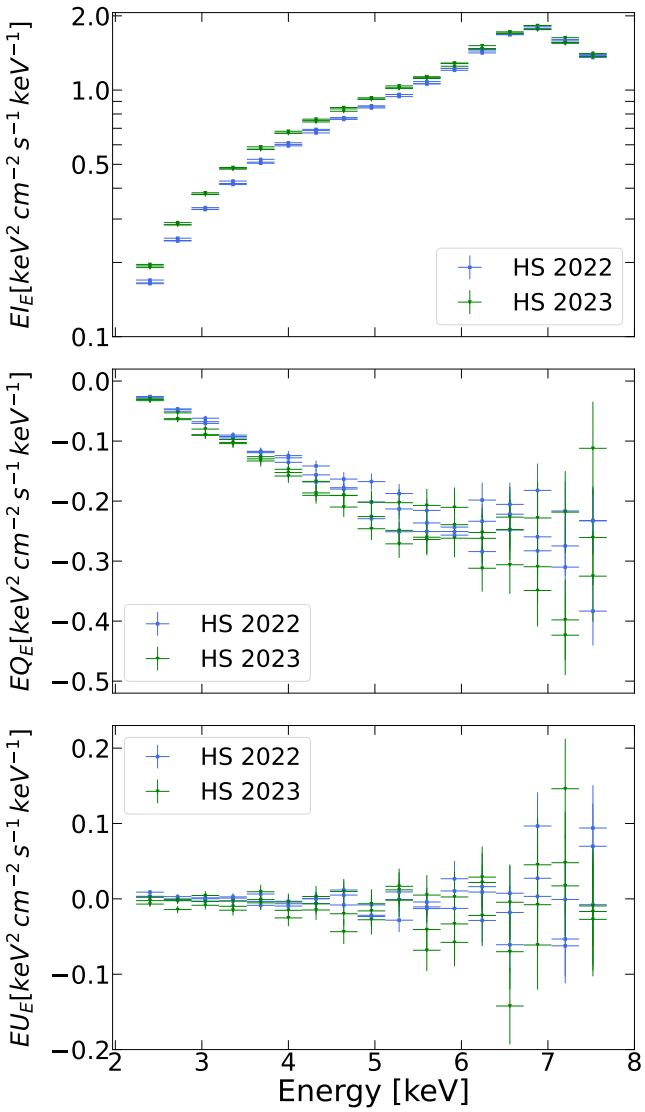

Figure 3. Top to bottom: unfolded EF_E (energy flux) spectra of Stokes I, Q, and U, comparing the spectral shape between HS 2022 (blue) and HS 2023 (green). Spectra are unfolded against a power law with photon index 1.7 for plotting purposes only.

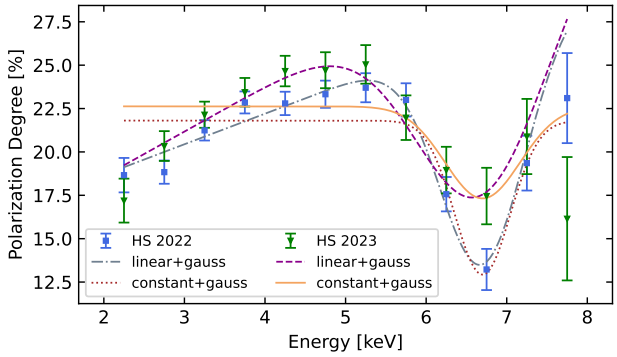

Figure 4. IXPE PDs (data points, HS 2022 in blue and HS 2023 in green) with two PD models fitted to the data of the two epochs: a linear change of the PD with energy plus a nonpolarized Gaussian is shown with the dashed–dotted gray line (HS 2022) and the dashed purple line (HS 2023). A constant PD model with a nonpolarized Gaussian is shown with the dotted brown line (HS 2022) and the solid orange line (HS 2023).

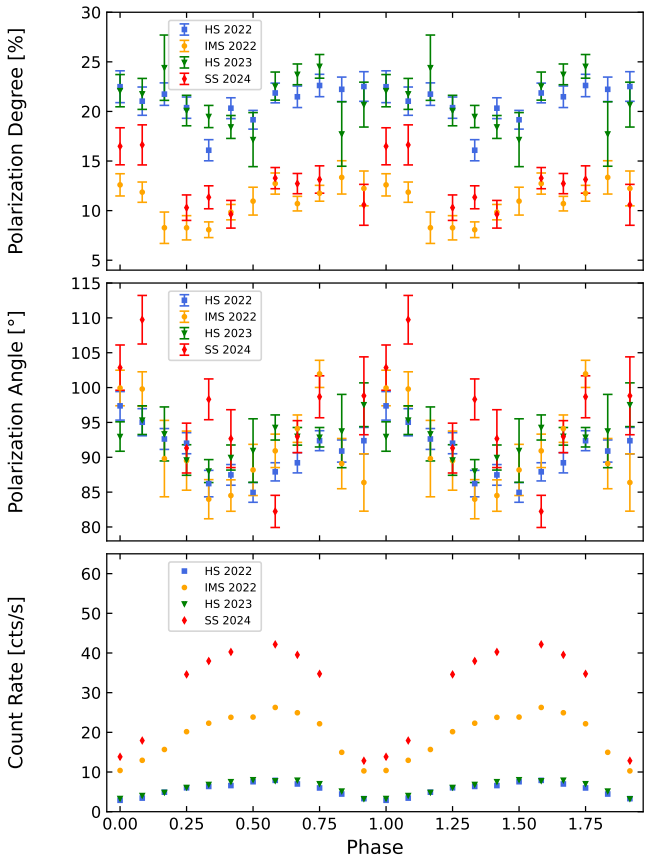

Figure 5. Dependence of the PD (top), PA (middle), and count rate (bottom) on the orbital phase. Each data point represents the mean value for a given orbital phase bin. HS 2022 in blue, IMS 2022 in yellow, HS 2023 in green, and SS 2024 in red.

3.3. Orbital Phase-resolved Polarimetry

A more intriguing view is offered when we examine the variation of polarization characteristics with the orbital phase of the source. Figure 5 demonstrates the connection between variation of polarimetric properties and count rate. The figure shows a strong orbital modulation of the PD and PA, similar to the previous result of A. Veledina et al. (2024a). The flux of the source varies systematically across its 4.8 hr orbital period. We also find notable changes in the polarimetric properties that are present in all four of the observations of Cyg X-3 performed by IXPE, having a cosine-like behavior. The flux modulation is consistent with the findings of I. I. Antokhin et al. (2022), while the corresponding modulation of the polarization properties suggests that the same orbital geometry also affects the observed polarization signal. This interpretation is supported by recent modeling of the orbitally modulated polarization, which demonstrates that the observed single-peaked variability can only be reproduced by an asymmetric, opaque scattering structure, likely associated with an intra-binary bow shock (V. Ahlberg et al. 2025). Specifically, I. I. Antokhin et al. (2022) showed that the X-ray light curves displayed a deep primary minimum at the superior conjunction of the compact object, followed by an asymmetric recovery and a secondary dip near phase ≈0.4.

The PD of HS 2023 varied between ∼17% and ∼25%, while PA underwent a modulation between ∼87° and ∼95°, coinciding with the variations observed during HS 2022 within the margin of error. These findings are further reinforced by a goodness-of-fit comparison between the constant versus cosine fits. The cosine function only has two free parameters (amplitude and offset), while the angular frequency is defined by the orbital period of the source, and the initial phase is fixed to 0. Seven out of eight datasets (one dataset of PD and one of PA, per each observation) show strong evidence ($\geqslant 3\sigma$) that the cosine model significantly outperforms the constant model. The PD during HS 2023 and the PA during IMS 2022 both show orbital variations at 4.1σ significance. The only case showing a moderate improvement in the fit at 2.3σ significance is the PA during SS 2024. The cosine-like modulation is consistent across all datasets, suggesting a genuine physical effect rather than statistical fluctuation.

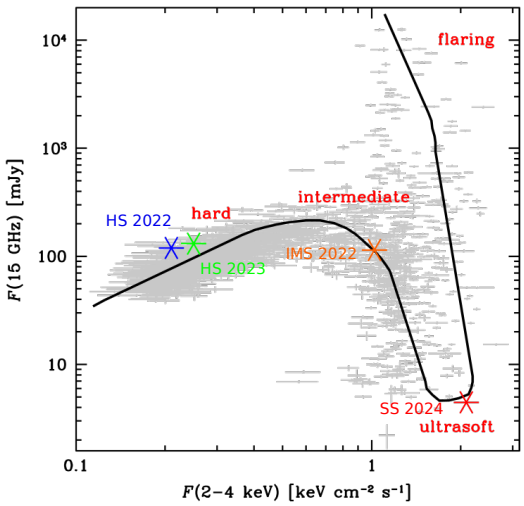

Figure 6. X-ray versus radio flux density diagram. Blue, orange, green, and red asterisks indicate the IXPE observations HS 2022, IMS 2022, HS 2023, and SS 2024, respectively. Gray points represent data from AMI and were presented in A. A. Zdziarski et al. (2016).

3.4. Radio–X-Ray Correlation

In order to better understand the spectral properties of the source, and to place the new HS 2023 observation in the broader spectral state context, we looked at the X-ray versus radio flux density diagram (Figure 6; using radio data from the Arcminute Microkelvin Imager, presented in A. A. Zdziarski et al. 2016) during the time of the IXPE observations. The source is typically found in the hard spectral state, as was the case for two out of the four IXPE observations (HS 2022 and HS 2023). It is not surprising, although somewhat rare, to see the source in an SS. Such a transition is typically accompanied by a rise in the soft X-ray flux and a decrease of radio emission (IMS 2022 and SS 2024). The inclusion of the HS 2023 point in this diagram shows that it follows the expected radio–X-ray correlation for the HS. Unlike the case of the polarimetric properties, where we have seen HS 2022 and HS 2023 to be almost identical, the spectral properties of these two observations are more diverse (e.g., Δ count rate $\leqslant 30\%$, or the spectral shape becomes notably different below $\sim$ 5 keV, as shown in the top panel of Figure 3), highlighting that similar polarization properties can arise despite noticeable spectral differences.

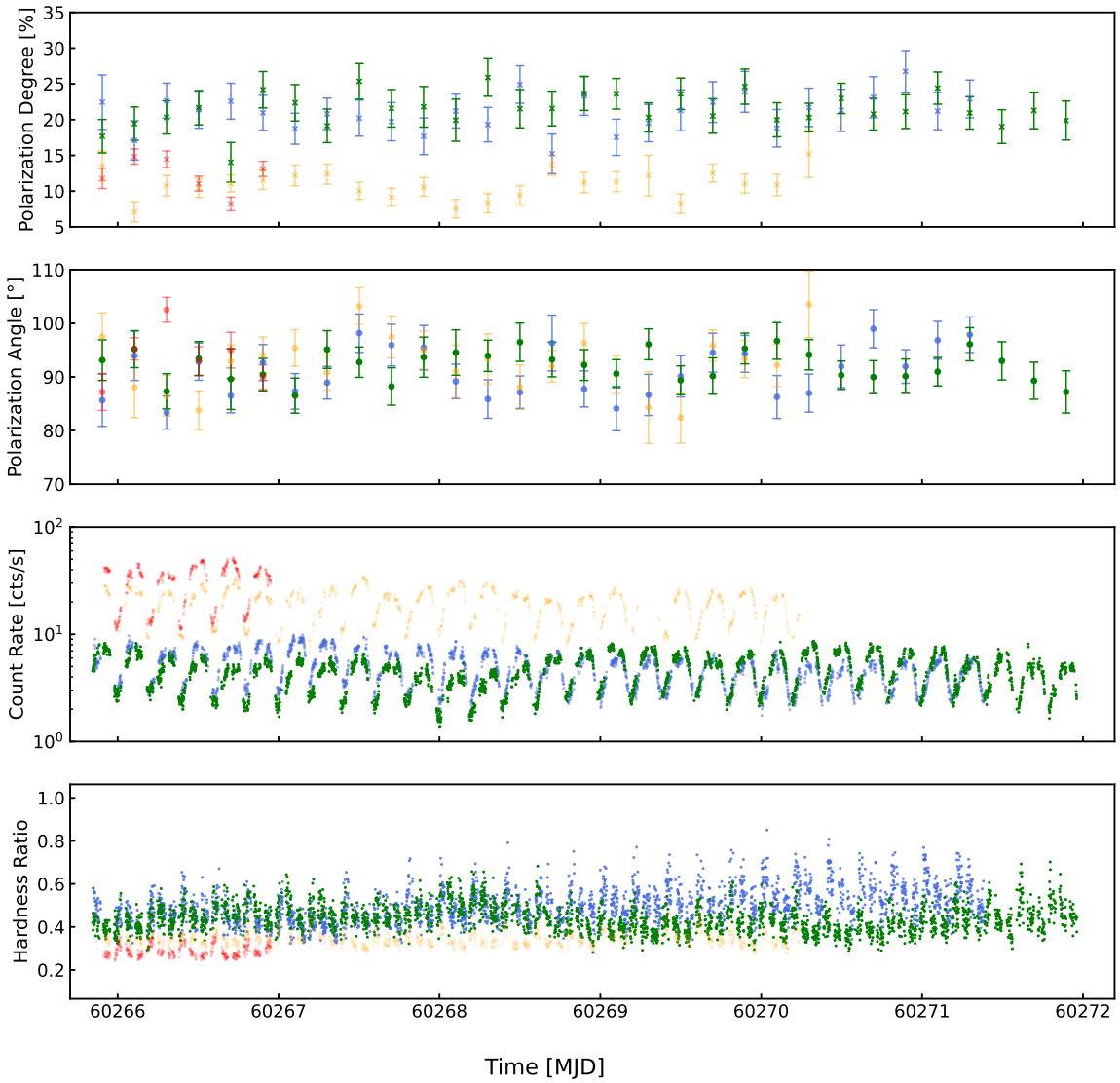

Figure 7. PD, PA, count rate, and hardness ratio (top to bottom) for HS 2022 (blue), IMS 2022 (yellow), HS 2023 (green), and SS 2024 (red) variation with time. HS 2022, IMS 2022, and SS 2024 are shifted for the first superior conjunction of the system during the IXPE observations to coincide with that of HS 2023. The entire 2–8 keV energy band was considered with data binned in intervals of 500 s. For HS 2022, only the first observational epoch is shown here, as the second epoch does not provide additional information beyond previous studies (A. Veledina et al. 2024a).

3.5. Time-dependent Orbit-average Analysis

We also study the temporal variations in the polarimetric and spectral properties, shown in Figure 7. The HS 2022 (blue), IMS 2022 (yellow), HS 2023 (green), and SS 2024 (red) observations were plotted so that their first superior conjunctions are aligned. For all four of these observations, we see orbital phase variations of the polarization properties, with the PD of IMS 2022 consistently below the PD of HS 2022 and HS 2023 during the entirety of the observation, while the PA stays stable between all four observations (the first and second panels from the top of Figure 7, respectively). The light curve (third panel from the top) clearly shows orbital variability over the observational period for all four observations. The orbit-average values show flux in the IMS and SS higher than in the two HSs by approximately 1 order of magnitude.

4. Summary

We find that both the time-average and orbital phase-resolved polarimetric properties of HS 2023 are remarkably similar to those of HS 2022, despite the fact that the observations were taken 11 months apart (considered from the end of HS 2022 to the start of HS 2023) with a flux difference of $\Delta\,\text{count rate} \leqslant 30\%$ and after the source had made an incursion into the IMS (Figures 1 and 5). Based on this finding, we can conclude that the geometry of the system is stable for these two IXPE observations, and, by extension, generally in the hard X-ray spectral state of the system: the primary X-ray source is covered by an optically thick envelope, and the emission escapes through the narrow funnel with the opening angle $\lesssim 15^\circ$, as was found for HS 2022 (A. Veledina et al. 2024a).

X-ray polarimetry observations of Cyg X-3 reveal that while the polarization properties in the HS 2022 and HS 2023 states are comparable, they show different spectral dependencies, with linear energy-dependent polarization models favored over constant polarization (improvements of $\sim 4\sigma$ and $\sim 3.5\sigma$, respectively). The data suggest a possible suppression of polarization at low energies observed in HS 2023, which could potentially result from a combination of effects, including a

possible contribution from emission lines, unpolarized reprocessed emission from funnel walls, or scattered light from the central source.

We find the HS 2023 orbit-average time-dependent polarization is constant, similar to HS 2022 (Figure 7). This contrasts with the higher spread of orbit-average values of PD in the IMS and SS, where we find marginal significance for time-dependent variations. This finding suggests that the polarization production mechanism remains stable in the HS and the geometry is not too sensitive to parameter variations. However, we note that only a single observation for each of the IMS and SS has been carried out with IXPE. Additional polarimetric observations in these states are needed to assess whether their geometries are similarly stable over time. Furthermore, observations of the source in the flaring state—the only spectral state not yet observed with IXPE—would provide valuable insights into the polarization behavior across the complete range of accretion states. This bolsters the earlier finding by A. Veledina et al. (2024a) that a small $\lesssim 15^\circ$ funnel opening angle is preferred over a larger $\sim 30^\circ$ funnel opening angle. This is because, although both opening angles give the same polarization, in the latter case, the PD is highly sensitive to variations in the opening angle on the scale of less than 1° (Figure 4(b) of A. Veledina et al. 2024a). While the influence of the funnel size and opening angle on the observed emission is now established, the role of other physical parameters of the funnel remains uncertain and requires further observational constraints.

Acknowledgments

The Imaging X-ray Polarimetry Explorer (IXPE) is a joint US and Italian mission. The US contribution is supported by the National Aeronautics and Space Administration (NASA) and led and managed by its Marshall Space Flight Center (MSFC), with industry partner Ball Aerospace (contract NNM15AA18C). The Italian contribution is supported by the Italian Space Agency (Agenzia Spaziale Italiana, ASI) through contract ASI-OHBI-2022-13-I.0, agreements ASI-INAF-2022-19-HH.1-2026 and ASI-INFN-2017.13-H0, and its Space Science Data Center (SSDC) with agreements ASI-INAF 2025-33-HH.0 and ASI-INFN 2026-5-HH.0, and by the Istituto Nazionale di Astrofisica (INAF) and the Istituto Nazionale di Fisica Nucleare (INFN) in Italy. This research used data products provided by the IXPE Team (MSFC, SSDC, INAF, and INFN) and distributed with additional software tools by the High-Energy Astrophysics Science Archive Research Center (HEASARC) at NASA Goddard Space Flight Center (GSFC).

A.V. acknowledges support from the Academy of Finland grant 355672. Nordita is supported in part by NordForsk. A.A.Z. acknowledges support from the Polish National Science Center grants 2019/35/B/ST9/03944 and 2023/48/Q/ST9/00138. M. D. and J.S. thank GACR project 21-06825X for the support and institutional support from RVO:67985815. The work of G.M. is partially supported by the PRIN 2022—2022LWPEXW—"An X-ray view of compact objects in polarized light," CUP C53D23001180006. A.I. acknowledges support from the Royal Society. P.O.P. acknowledges financial support from the French Space National Agency (CNES) and the National Center of Scientific Research (CNRS) via its "Action Thématique" PEM. J.P. acknowledges institutional support from RVO:67985815. I.L. was funded by the European Union ERC-2022-STG-BOOTES-101076343. Views and opinions expressed are, however, those of the author(s) only and do not necessarily reflect those of the European Union or the European Research Council Executive Agency. Neither the European Union nor the granting authority can be held responsible for them.

ORCID iDs

Romana Mikušincová https://orcid.org/0000-0001-7374-843X
Alexandra Veledina https://orcid.org/0000-0002-5767-7253
Fabio Muleri https://orcid.org/0000-0003-3331-3794
Raul Ciancarella https://orcid.org/0009-0009-3289-3767
Andrzej Zdziarski https://orcid.org/0000-0002-0333-2452
David A. Green https://orcid.org/0000-0003-3189-9998
Michael McCollough https://orcid.org/0000-0002-8384-3374
Henric Krawczynski https://orcid.org/0000-0002-1084-6507
James F. Steiner https://orcid.org/0000-0002-5872-6061
Michal Dovčiak https://orcid.org/0000-0003-0079-1239
Varpu Ahlberg https://orcid.org/0009-0006-9714-5063
Stefano Bianchi https://orcid.org/0000-0002-4622-4240
Alessandro Di Marco https://orcid.org/0000-0003-0331-3259
Javier A. García https://orcid.org/0000-0003-3828-2448
Adam Ingram https://orcid.org/0000-0002-5311-9078
Philip Kaaret https://orcid.org/0000-0002-3638-0637
Timothy Kallman https://orcid.org/0000-0002-5779-6906
Hu Kun https://orcid.org/0000-0002-9705-7948
Fabio La Monaca https://orcid.org/0000-0001-8916-4156
Alexander Lange https://orcid.org/0000-0003-3540-2870
Vladislav Loktev https://orcid.org/0000-0001-6894-871X
Guglielmo Mastroserio https://orcid.org/0000-0003-4216-7936
Giorgio Matt https://orcid.org/0000-0002-2152-0916
Razieh Emami https://orcid.org/0000-0002-2791-5011
Pierre-Olivier Petrucci https://orcid.org/0000-0001-6061-3480
Jakub Podgorný https://orcid.org/0000-0001-5418-291X
Juri Poutanen https://orcid.org/0000-0002-0983-0049
Ajay Ratheesh https://orcid.org/0000-0003-0411-4243
Nicole Rodriguez https://orcid.org/0000-0001-5256-0278
Jiří Svoboda https://orcid.org/0000-0003-2931-0742
Francesco Tombesi https://orcid.org/0000-0002-6562-8654
Iván Agudo https://orcid.org/0000-0002-3777-6182
Lucio A. Antonelli https://orcid.org/0000-0002-5037-9034
Matteo Bachetti https://orcid.org/0000-0002-4576-9337
Luca Baldini https://orcid.org/0000-0002-9785-7726
Wayne H. Baumgartner https://orcid.org/0000-0002-5106-0463
Ronaldo Bellazzini https://orcid.org/0000-0002-2469-7063
Stephen D. Bongiorno https://orcid.org/0000-0002-0901-2097
Raffaella Bonino https://orcid.org/0000-0002-4264-1215
Alessandro Brez https://orcid.org/0000-0002-9460-1821
Niccolò Bucciantini https://orcid.org/0000-0002-8848-1392
Fiamma Capitanio https://orcid.org/0000-0002-6384-3027
Simone Castellano https://orcid.org/0000-0003-1111-4292
Elisabetta Cavazzuti https://orcid.org/0000-0001-7150-9638
Chien-Ting Chen https://orcid.org/0000-0002-4945-5079
Stefano Ciprini https://orcid.org/0000-0002-0712-2479
Enrico Costa https://orcid.org/0000-0003-4925-8523
Alessandra De Rosa https://orcid.org/0000-0001-5668-6863
Ettore Del Monte https://orcid.org/0000-0002-3013-6334
Laura Di Gesu https://orcid.org/0000-0002-5614-5028
Niccolò Di Lalla https://orcid.org/0000-0002-7574-1298

Immacolata Donnarumma https://orcid.org/0000-0002-4700-4549
Victor Doroshenko https://orcid.org/0000-0001-8162-1105
Steven R. Ehlert https://orcid.org/0000-0003-4420-2838
Teruaki Enoto https://orcid.org/0000-0003-1244-3100
Yuri Evangelista https://orcid.org/0000-0001-6096-6710
Sergio Fabiani https://orcid.org/0000-0003-1533-0283
Riccardo Ferrazzoli https://orcid.org/0000-0003-1074-8605
Shuichi Gunji https://orcid.org/0000-0002-5881-2445
Jeremy Heyl https://orcid.org/0000-0001-9739-367X
Wataru Iwakiri https://orcid.org/0000-0002-0207-9010
Svetlana G. Jorstad https://orcid.org/0000-0001-6158-1708
Vladimir Karas https://orcid.org/0000-0002-5760-0459
Fabian Kislat https://orcid.org/0000-0001-7477-0380
Jeffery J. Kolodziejczak https://orcid.org/0000-0002-0110-6136
Luca Latronico https://orcid.org/0000-0002-0984-1856
Ioannis Liodakis https://orcid.org/0000-0001-9200-4006
Simone Maldera https://orcid.org/0000-0002-0698-4421
Alberto Manfreda https://orcid.org/0000-0002-0998-4953
Frédéric Marin https://orcid.org/0000-0003-4952-0835
Andrea Marinucci https://orcid.org/0000-0002-2055-4946
Alan P. Marscher https://orcid.org/0000-0001-7396-3332
Herman L. Marshall https://orcid.org/0000-0002-6492-1293
Francesco Massaro https://orcid.org/0000-0002-1704-9850
Ikuyuki Mitsuishi https://orcid.org/0000-0002-9901-233X
Tsunefumi Mizuno https://orcid.org/0000-0001-7263-0296
Michela Negro https://orcid.org/0000-0002-6548-5622
Chi- Yung Ng https://orcid.org/0000-0002-5847-2612
Stephen L. O'Dell https://orcid.org/0000-0002-1868-8056
Nicola Omodei https://orcid.org/0000-0002-5448-7577
Chiara Oppedisano https://orcid.org/0000-0001-6194-4601
Alessandro Papitto https://orcid.org/0000-0001-6289-7413
George G. Pavlov https://orcid.org/0000-0002-7481-5259
Abel L. Peirson https://orcid.org/0000-0001-6292-1911
Matteo Perri https://orcid.org/0000-0003-3613-4409
Melissa Pesce-Rollins https://orcid.org/0000-0003-1790-8018
Maura Pilia https://orcid.org/0000-0001-7397-8091
Andrea Possenti https://orcid.org/0000-0001-5902-3731
Simonetta Puccetti https://orcid.org/0000-0002-2734-7835
Brian D. Ramsey https://orcid.org/0000-0003-1548-1524
John Rankin https://orcid.org/0000-0002-9774-0560
Oliver J. Roberts https://orcid.org/0000-0002-7150-9061
Roger W. Romani https://orcid.org/0000-0001-6711-3286
Carmelo Sgrò https://orcid.org/0000-0001-5676-6214
Patrick Slane https://orcid.org/0000-0002-6986-6756
Paolo Soffitta https://orcid.org/0000-0002-7781-4104
Gloria Spandre https://orcid.org/0000-0003-0802-3453
Douglas A. Swartz https://orcid.org/0000-0002-2954-4461
Toru Tamagawa https://orcid.org/0000-0002-8801-6263
Fabrizio Tavecchio https://orcid.org/0000-0003-0256-0995
Roberto Taverna https://orcid.org/0000-0002-1768-618X
Allyn F. Tennant https://orcid.org/0000-0002-9443-6774
Nicholas E. Thomas https://orcid.org/0000-0003-0411-4606
Alessio Trois https://orcid.org/0000-0002-3180-6002
Sergey S. Tsygankov https://orcid.org/0000-0002-9679-0793
Roberto Turolla https://orcid.org/0000-0003-3977-8760
Jacco Vink https://orcid.org/0000-0002-4708-4219
Martin C. Weisskopf https://orcid.org/0000-0002-5270-4240
Kinwah Wu https://orcid.org/0000-0002-7568-8765
Fei Xie https://orcid.org/0000-0002-0105-5826
Silvia Zane https://orcid.org/0000-0001-5326-880X

References

Abdo, A. A., Ackermann, M., Ajello, M., et al. 2009, Sci, 326, 1512
Ahlberg, V., Bocharova, A., & Veledina, A. 2025, A&A, 704, A127
Antokhin, I. I., & Cherepashchuk, A. M. 2019, ApJ, 871, 244
Antokhin, I. I., Cherepashchuk, A. M., Antokhina, E. A., & Tatarnikov, A. M. 2022, ApJ, 926, 123
Atwood, W. B., Abdo, A. A., Ackermann, M., et al. 2009, ApJ, 697, 1071
Audard, M., Awaki, H., Ballhausen, R., et al. 2024, ApJL, 977, L34
Baldini, L., Bucciantini, N., Lalla, N. D., et al. 2022, SoftX, 19, 101194
Beloborodov, A. M. 1998, ApJL, 496, L105
Cerutti, B., Dubus, G., Malzac, J., et al. 2011, A&A, 529, A120
Corbel, S., Dubus, G., Tomsick, J. A., et al. 2012, MNRAS, 421, 2947
Di Marco, A., Costa, E., Muleri, F., et al. 2022, AJ, 163, 170
Di Marco, A., Soffitta, P., Costa, E., et al. 2023, AJ, 165, 143
Dovčiak, M., Podgorný, J., Svoboda, J., et al. 2024, Galax, 12, 54
Dubus, G., Cerutti, B., & Henri, G. 2010, MNRAS, 404, L55
Ewing, M., Parra, M., Mastroserio, G., et al. 2025, MNRAS, 541, 1774
Giacconi, R., Gorenstein, P., Gursky, H., & Waters, J. R. 1967, ApJL, 148, L119
Gregory, P. C., Kronberg, P. P., Seaquist, E. R., et al. 1972, Natur, 239, 440
Hjalmarsdotter, L., Zdziarski, A. A., Larsson, S., et al. 2008, MNRAS, 384, 278
Hjalmarsdotter, L., Zdziarski, A. A., Szostek, A., & Hannikainen, D. C. 2009, MNRAS, 392, 251
Ingram, A., Bollemeijer, N., Veledina, A., et al. 2024, ApJ, 968, 76
Kallman, T., McCollough, M., Koljonen, K., et al. 2019, ApJ, 874, 51
Kravtsov, V., Bocharova, A., Veledina, A., et al. 2025, A&A, 701, A115
Krawczynski, H., & Hu, K. 2025, ApJ, 993, 54
Krawczynski, H., Muleri, F., Dovčiak, M., et al. 2022, Sci, 378, 650
McCollough, M. L., Robinson, C. R., Zhang, S. N., et al. 1999, ApJ, 517, 951
Miura, D., Yamaguchi, H., & Ballhausen, R. 2025, PASJ, 77, psaf057
Parsignault, D. R., Gursky, H., Kellogg, E. M., et al. 1972, NPhS, 239, 123
Piano, G., Tavani, M., Vittorini, V., et al. 2012, A&A, 545, A110
Podgorný, J., Svoboda, J., Dovčiak, M., et al. 2024, A&A, 686, L12
Poutanen, J., Veledina, A., & Beloborodov, A. M. 2023, ApJL, 949, L10
Reid, M. J., & Miller-Jones, J. C. A. 2023, ApJ, 959, 85
Soffitta, P., Baldini, L., Bellazzini, R., et al. 2021, AJ, 162, 208
Spencer, R. E., Garrett, M., Bray, J. D., & Green, D. A. 2022, MNRAS, 512, 2618
Szostek, A., Zdziarski, A. A., McCollough, M. L., et al. 2008, MNRAS, 388, 1001
Tavani, M., Bulgarelli, A., Piano, G., et al. 2009, Natur, 462, 620
Trushkin, S., McCollough, M., Nizhelskij, N., & Tsybulev, P. 2017, Galax, 5, 86
Ursini, F., Marinucci, A., Matt, G., et al. 2023, MNRAS, 519, 50
van Kerkwijk, M. H., Geballe, T. R., King, D. L., van der Klis, M., & van Paradijs, J. 1996, A&A, 314, 521
Veledina, A., Muleri, F., Dovčiak, M., et al. 2023, ApJL, 958, L16
Veledina, A., Muleri, F., Poutanen, J., et al. 2024a, NatAs, 8, 1031
Veledina, A., Poutanen, J., Bocharova, A., et al. 2024b, A&A, 688, L27
Weisskopf, M. C., Soffitta, P., Baldini, L., et al. 2022, JATIS, 8, 026002
Zdziarski, A. A., Mikolajewska, J., & Belczynski, K. 2013, MNRAS, 429, L104
Zdziarski, A. A., Segreto, A., & Pooley, G. G. 2016, MNRAS, 456, 775